The Effect of Pulse Shape on Laser Imprinting and Beam Smoothing

Inertial confinement fusion (ICF) targets are inherently hydrodynamically unstable;[1–3] as a result, perturbations in the target shell can grow exponentially because of Rayleigh–Taylor (RT) instability.[4] For high-convergence implosions it is important to minimize target perturbations and their growth. In direct-drive ICF, nonuniformities in the drive laser produce pressure perturbations that cause mass and velocity perturbations in the target. These "imprinted" perturbations seed the RT instability and ultimately disrupt the implosion. To minimize imprinting, the drive laser must be as uniform as possible. This requires complex laser beam–smoothing techniques.[5] In many ICF target designs the temporal shape of the drive is determined by compression hydrodynamics and thermodynamics (stability and isentrope) and not necessarily to minimize imprint. It is therefore important that the effect of temporal pulse shape on imprinting and beam smoothing be measured and understood. Various experiments have measured imprinting[6–12] and have used control perturbations to normalize the results.[10,12] The experiments reported here are the first to demonstrate the pulse shape's effect on imprinting.

A series of experiments on the OMEGA laser system[13] measured imprinting efficiency using preimposed modulations on planar targets to calibrate the imprint level. The imprinting produced by different temporal pulse shapes and beam-smoothing techniques is compared. Rapidly rising (~100 ps/decade) pulses produce less imprint than pulses with ~1-ns rise time when no temporal beam smoothing is employed. Furthermore, the effect of smoothing by spectral dispersion (SSD)[5] is less pronounced for these rapid-rise pulses. These observations are consistent with plasma smoothing[14] by thermal conduction and differences in the rate at which each pulse produces plasma early in the laser–target interaction.

Imprinting occurs when drive nonuniformities produce pressure perturbations at the target surface that, in turn, produce velocity and mass perturbations at the ablation surface where the RT instability occurs. Laser energy is absorbed in the region outside the critical surface and conducted axially to the ablation surface. If sufficient depth of plasma is present, lateral thermal conduction can provide smoothing of the deposition nonuniformities, thus ending imprinting.[14] Previous simulations[15,16] have investigated imprinting and have indicated that, for a given laser wavelength, imprint efficiency depends linearly on $\delta I/I$ for the intensities relevant to ICF (i.e., $\delta m \propto \delta I/I$), but the duration of imprinting varies depending on the plasma smoothing. Numerical simulations described below show that the condition for smoothing a perturbation of wavelength k is that $kd_c \sim 2$, where d_c is the distance between the ablation surface and a central location in the energy deposition profile.[10] As that thermal conduction region grows, longer wavelengths can be smoothed; thus, for each wavelength the duration of laser imprinting and its total magnitude depends on the time to develop a sufficiently sized conduction zone. Since a slowly rising pulse produces a plasma at a slower rate, imprinting occurs over a longer time, resulting in a higher imprint level in the absence of beam smoothing. The plasma formation rate therefore affects the wavelength dispersion of smoothing. For a given wavelength of interest, imprinting ultimately ceases when the conduction region grows to a sizable fraction of that wavelength. When kd_c is about 2, d_c is about one-third the wavelength of the perturbation. To check the wavelength dependence, the imprint levels of both 30- and 60-μm wavelengths were measured. These correspond to ℓ-modes of 50 and 100 on mm-sized targets, which are pertinent to direct-drive ICF and are in the linear RT growth regime during these measurements.

In these experiments, 20-μm-thick CH (ρ = 1.05 g/cm^3) targets with preimposed modulations were irradiated at 2×10^{14} W/cm^2 by six overlapping UV beams from the OMEGA laser. Target nonuniformities were measured using through-foil x-ray radiography.[17] Experiments were performed with two laser pulse shapes: a 3-ns square (in time) pulse and a 3-ns ramp pulse. The square pulse had a rise time of 100 ps per decade of intensity and an intensity of 2×10^{14} W/cm^2. The ramp pulse rose linearly from ~10^{13} to 2.5×10^{14} W/cm^2 in 3 ns. The latter pulse had a 100 ps/decade

rise to ~10^{13} W/cm^2 before the ramp commenced. For each pulse shape, experiments were performed with and without 2-D SSD beam smoothing.

The driven targets were backlit with x rays produced by a uranium backlighter irradiated at 2×10^{14} W/cm^2 (with 11 additional beams). X rays transmitted through the target and a 3-μm-thick Al blast shield were imaged by a framing camera with 8-μm pinholes filtered with 20 μm of Be and 6 μm of Al. This yielded the highest sensitivity for average photon energy of ~1.3 keV.[17] The framing camera produced eight temporally distinct images of ~100-ps duration and a magnification of 12. The use of optical fiducial pulses, coupled with an electronic monitor of the framing-camera output, provided a frame-timing precision of about 70 ps.

Unfortunately laser imprint cannot easily be measured directly, so measurements often rely on some level of RT growth to produce detectable signals. Targets with low-amplitude, single-mode initial perturbations are used here to provide a calibration from which the initial amplitude of laser imprinting was determined. The basis of this calibration is that in the linear regime the imprinted perturbations ultimately experience similar unstable RT growth to those of preimposed modulations.[8] Although imprinting also produces velocity perturbations, it is useful to assign an equivalent surface roughness to imprinting. This "mass equivalence" is used as a measure of the imprint. The mass equivalence is found by extrapolating the temporal evolution of the imprinted amplitudes back to $t = 0$ by measuring the ratio of the amplitudes of the imprinted and preimposed modes after RT growth has occurred. This requires that the RT instability for those modes remain in the linear regime and do not experience saturation or nonlinear effects.[18] Saturation of RT growth is discussed at length in Ref. 19, where it was shown that at $\lambda = 60$ μm, both the single-mode and the imprinted perturbations behaved linearly for our experimental conditions and observation times. The 30-μm-wavelength imprinting data was measured before the onset of saturation.[19]

The mass equivalence[15] for a specific wave number can be defined as

$$A_{\text{eq}}(k,0) = \left[A_{\text{imprint}}(k,t)/A_{\text{pre}}(k,t)\right]A_{\text{pre}}(k,0), \qquad (1)$$

where $A_{\text{imprint}}(k,t)$ is the measured amplitude of the imprinted features, $A_{\text{pre}}(k,t)$ is the measured amplitude of the preimposed modulation, and $A_{\text{pre}}(0)$ is the known initial amplitude of the preimposed modulation. Using the measurements of the laser nonuniformity, a measure of imprint efficiency[15] is defined as

$$\eta_i(k) = \frac{A_{\text{eq}}(k,0)}{(\delta I/I)},$$

where $\delta I/I$ is the fractional irradiation nonuniformity at the same wavelength.

The amplitudes of these perturbations are obtained using a Fourier analysis of the radiographed images. The Fourier amplitude of the imprint at a given wavelength is defined as the rms of all mode amplitudes at that wavelength, i.e., those modes at a given radius (centered at zero frequency) in frequency space. (The contribution of the preimposed modulation is not included.) The values are summed in quadrature because they are expected to be uncorrelated since they result from the random speckle in the laser. The analysis box is 300 μm in the target plane; thus, in Fourier space, the pixel size is 3.3 mm^{-1}. The pixels at radius 5±0.5 provide the amplitudes of modes with wavelengths between 55 μm and 67 μm, and those at 10±0.5 pixels provide amplitudes for wavelengths between 29 μm and 32 μm.

The preimposed single-mode modulations are two dimensional and possess localized features along a single axis in the Fourier plane at the spatial frequency of this modulation. Figure 80.12(a) depicts a typical radiographic image from these experiments; note that the vertical preimposed modulations are just visible in the mottled pattern produced by the laser imprint. The 2-D Fourier transform of this image after Weiner filtering[17] is shown as a surface plot in Fig. 80.12(b), where the signals from the preimposed modulations stand out from the broadband imprinted features that populate most of the 2-D Fourier space. Figure 80.12(c) depicts a one-pixel-wide annulus that illustrates how the amplitudes for the imprinting are measured. The ratio of the rms value of these amplitudes to that of the preimposed mode times the initial amplitude is used to determine the mass equivalence of imprinting of the control mode. (The box size is optimized for the preimposed mode, thereby ensuring that all the power in that mode is contained in the single pixel.)

For these experiments a variety of beam-smoothing techniques were used. A single-beam laser with only a distributed phase plate (DPP)[20] and no SSD provides a static speckle pattern with ~80% to 100% nonuniformity in wavelengths from 2 μm to 250 μm.[21] The overlap of six beams reduces this

nonuniformity by ~ $\sqrt{6}$. SSD provides a time-varying reduction of the nonuniformity by continually shifting the DPP pattern on the target. The smoothing rate and the asymptotic smoothing level depend on the 2-D SSD bandwidth, which in this experiment is $\Delta\nu = 0.2\ \mathrm{THz}_{\mathrm{UV}}$. In some cases, distributed polarization rotators (DPR's)[22] were added. These provide an instantaneous $\sqrt{2}$ reduction of nonuniformity[23] by separating each beam into two orthogonally polarized beams that are separated by 80 μm in the target plane.

Figure 80.13 shows the measured mass equivalence (in μm) of imprinting at 60-μm wavelength for all three smoothing conditions for the 3-ns square pulse in a series of shots with similar drive intensities. The temporal axis shows the time at which each frame was taken. The mass-equivalence data separate into distinct sets associated with each uniformity condition and are constant in time. Both observations are expected and confirm the utility of this technique. When the growth of the imprinted features are in the linear regime, they should remain a constant ratio of the amplitude of the preimposed mode, leading to a constant mass equivalence. This quantity's dependence on the initial uniformity produced by the various beam-smoothing techniques indicates the sensitivity of this method. For example, the addition of DPR's to the SSD experiments (open squares) reduces the mass equivalence by the expected factor of $\sqrt{2}$ (shaded squares).

The pulse shape's effect on imprinting was then studied by repeating these measurements with a slowly rising pulse, i.e., with an ~2.5-ns rise to the maximum intensity. Figure 80.14 shows the deduced mass equivalence as a function of time for the two pulse shapes, each with and without SSD. Again the data group according to laser conditions (pulse shape or SSD) and exhibit an approximately constant value over considerable times.

These data show that without SSD the ramp pulse produces about 50% more imprinting (higher mass equivalence) than the square pulse. They also indicate that although SSD produces a greater reduction of imprinting on the ramp pulse, the net imprint level after SSD is about the same for both pulses.

Similar experiments were performed using preimposed modulations with $\lambda = 30\ \mu$m. Table 80.I lists the mass-equivalence results for all the experiments. In addition, the imprint efficiency was calculated for the experiments without SSD using the irradiation nonuniformities reported in Ref. 19. The uniformity results were scaled by the differences in analysis boxes between the radiography ($L = 300\ \mu$m; $\Delta k = 0.021$) and the optical experiments ($L = 440\ \mu$m; $\Delta k = 0.0143$). In addition, the values obtained in Ref. 19 were reduced by $\sqrt{6}$ since these experiments utilized six beams. Thus, $\delta I/I$ was 0.00684 for 30 μm and 0.00493 for 60 μm. Lastly, a factor of 2 was included to relate the complex amplitude for ΔI to the mass equivalence, which was normalized to a real cosine function. Since the SSD produces time-varying uniformity, it is difficult to assign a single number to the uniformity and hence the imprint efficiency is not calculated.

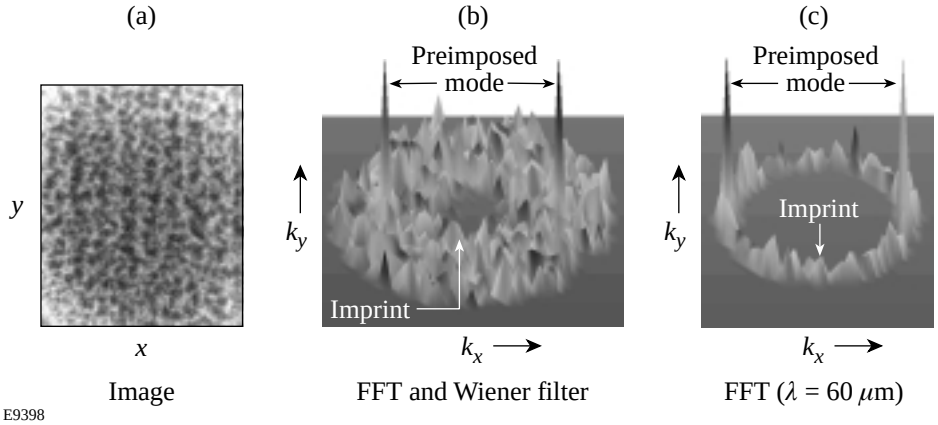

Figure 80.12
(a) Sample of an x-ray radiograph of a target with preimposed 60-μm-wavelength perturbations (vertical striations). The mottled pattern throughout the image is caused by the imprinted features. (b) Representation of the Fourier spectrum of the image in (a), showing the broadband imprinted features as well as two peaks from the preimposed single-mode modulations. (c) The annulus at 55 μm to 68 μm containing two components: the preimposed modulations and the imprinted features. The latter is used as a control feature to gauge the initial amplitude of the imprinted features.

As discussed above, thermal smoothing in the plasma ultimately terminates laser imprint. The duration of imprinting, then, depends on the time required to produce sufficient plasma atmosphere to enable smoothing. One would expect that, compared to the square pulse, the ramp pulse should imprint for a longer duration because the ramp pulse delivers energy at a slower rate and the smoothing plasma is produced more slowly, leading to larger mass equivalence. The imprint efficiencies measured here are lower than those observed by Glendinning *et al.*[12] for a slower rise and lower-intensity ramp pulse, as expected.

Simulations of the experiments were performed with the 2-D hydrodynamics code *ORCHID*[24] to determine the predicted imprint efficiency and the time that pressure perturbations at the ablation surface become negligible as the result of plasma smoothing. The imprint efficiencies were calculated by imposing a single-mode nonuniformity in the laser irradiation. The evolution of the resulting perturbations was compared to that of preimposed mass perturbations of the same wavelength. The experimental temporal pulse shapes were used in the simulations. The simulation results shown in Table 80.I are in reasonable agreement with the measured

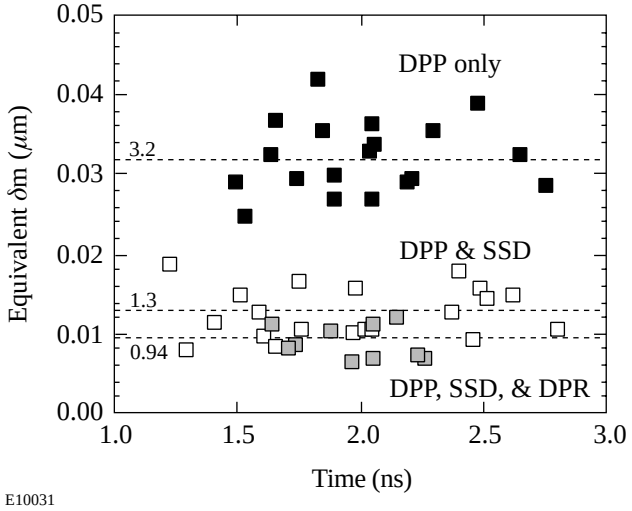

Figure 80.13
The mass equivalence (at 60 μm) derived from planar targets driven by laser beams having a 3-ns square pulse and three types of beam smoothing applied: DPP only (solid), DPP + SSD (open), and DPP + SSD + DPR (shaded). Note that the data segregate according to the laser nonuniformity. The mass equivalence is a measure of the total amount of imprinting, which is seen to decrease as greater beam smoothing is applied.

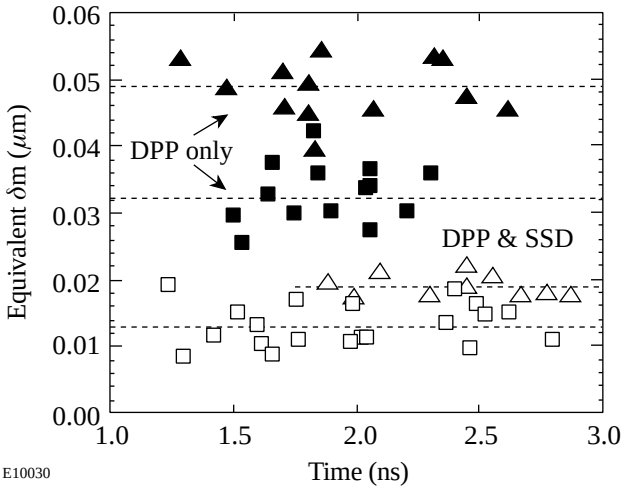

Figure 80.14
The deduced mass equivalence of the imprinted features (at 60 μm) for two pulse shapes: 3-ns square (squares) and ramp (triangles). These data show that for the same laser nonuniformity, a ramp pulse produces more imprinting. The solid and open symbols correspond, respectively, to each of the pulses without and with 2-D SSD. They indicate that the effect of SSD is greater for the ramp pulse, but the net imprint level is similar for the two pulses.

Table 80.I: Mass equivalence and imprint efficiency for various conditions.

Pulse-Shape Uniformity	Mass Equivalence (μm)		Imprint Efficiency: $\delta m/(\delta I/I)$ (μm)			
			Experiment		Simulation	
	60 μm	30 μm	60 μm	30 μm	60 μm	30 μm
Square (no SSD)	0.032±0.005	0.022±0.004	3.3±0.04	1.6±0.03	1.7	1.1
Ramp (no SSD)	0.049±0.008	0.023±0.005	5.0±0.06	1.7±0.04	3.1	2.3
Square (SSD)	0.013±0.003	0.010±0.003				
Ramp (SSD)	0.017±0.005	0.011±0.004				

values. Similar imprint efficiencies were calculated with the 2-D hydrodynamics code *LEOR*.[25] The 2-D simulations underestimate the efficiency at 60 μm, similar to the observations of Glendinning *et al.*[12]

The inherent surface roughness of these foils (transverse to the imposed modulations) was measured to be less than 1% of the imposed mode and, therefore, does not contribute significantly to the error in these measurements. One must consider, however, that the measured signal for the preimposed mode also has a contribution from the imprinted signal at that distinct mode. Since the relative phase of these two signals is arbitrary, the resultant signal can vary significantly when the imprint is a sizable fraction of the preimposed mode, as it is in the no-SSD cases.

Figure 80.15 shows the amplitude of the pressure perturbations (solid curves) at the ablation surface as a function of time for two cases: a ramp pulse and a square pulse, both without SSD. In these simulations a static 60-μm spatial-intensity perturbation of 5% was imposed on the irradiation intensity. Note that the smoothing rate is slower for the ramp pulse and the perturbations persist for a longer period. The temporal evolution (dashed curves) of the conduction zone (d_c) for the two pulse shapes is also shown. This is defined as the distance between the ablation surface and the mean of the energy deposition profile as weighted by a diffusion length: e^{-kz}.

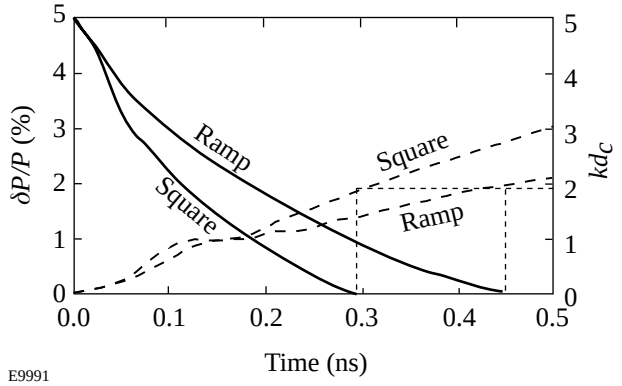

Figure 80.15
The amplitude of perturbations (solid lines) in the ablation pressure (at the ablation surface) as a function of time. The size of the conduction zone (dashed lines) as a function of time in CH targets driven by the square and ramp pulses.These graphs show that imprinting should stop at 300 ps for the square pulse and 450 ps for the ramp pulse. Note that for the square pulse the pressure perturbations are smoothed in 300 ps while for the ramp pulse this occurs at 450 ps.

Imprinting is expected to cease when pressure perturbations at the ablation surface are reduced to negligible levels. Figure 80.15 shows that this occurs for both pulse shapes when d_c ~2. Simple considerations of the distance between critical and ablation surfaces are insufficient to explain the behavior of the two pulses; rather the energy deposition profiles must also be accounted for because considerable smoothing can take place in the plasma region outside the critical surface.

When 2-D SSD is employed, the uniformity at $t = 0$ is the same as without SSD and reduces rapidly in time as $1/\nu$, where ν is the laser bandwidth. For these experiments the UV bandwidth is ~0.2 THz. While at this bandwidth the asymptotic smoothing level for 60 μm is reached in ~1.2 ns,[21] considerable smoothing occurs in less than 400 ps. The experimental results are consistent with this since SSD reduces the imprint for both pulse shapes, although there is greater reduction for the ramp pulse. Since imprinting in the ramp pulse lasts longer, SSD is able to provide greater benefit. The resulting imprint is similar for both pulses with SSD because the effective smoothing time for SSD is shorter than the duration of imprinting for both pulse shapes. Thus, significant SSD smoothing occurs before a large-enough conduction zone is produced. The calculated reduction of the mass equivalence with SSD present is somewhat larger (~60%) than the experimental observations.

This work has shown that for identical nonuniformities, the imprint level depends on the pulse shape, as expected. The total imprinting depends on the irradiation nonuniformity, the imprint efficiency, and the duration of imprint. Since the latter varies with pulse shape and other laser conditions, imprint efficiency cannot be considered invariant. These quantities are also laser wavelength dependent.[10,11] In addition, other processes such as shinethrough and laser–plasma instabilities (filamentation) could alter the intensity distribution within the plasma.

Preimposed modulations have been used as a reference to determine the mass equivalence of features imprinted by a drive laser. This technique behaves linearly under the experimental conditions described here. Slowly rising pulses produce more imprint and experience more smoothing because of SSD than steeply rising pulses. This is a result of the different rates at which smoothing plasma is initially formed, which ultimately determines the duration of imprinting. Numerical simulations confirm this physical picture and yield imprint efficiencies in reasonable agreement with the measured values.

ACKNOWLEDGMENT

This work was supported by the U.S. Department of Energy Office of Inertial Confinement Fusion under Cooperative Agreement No. DE-FC03-92SF19460, the University of Rochester, and the New York State Energy Research and Development Authority. The support of DOE does not constitute an endorsement by DOE of the views expressed in this article

REFERENCES

1. J. Nuckolls *et al.*, Nature **239**, 139 (1972).
2. J. D. Lindl, Phys. Plasmas **2**, 3933 (1995).
3. S. E. Bodner *et al*., Phys. Plasmas **5**, 1901 (1998).
4. G. Taylor, Proc. R. Soc. London, Ser. A **201**, 192 (1950); Lord Rayleigh, Proc. London Math. Soc. **XIV**, 170 (1883).
5. S. Skupsky and R. S. Craxton, Phys. Plasmas **6**, 2157 (1999).
6. M. Desselberger *et al.*, Phys. Rev. Lett. **68**, 1539 (1992).
7. D. H. Kalantar, M. H. Key, L. B. DaSilva, S. G. Glendinning, J. P. Knauer, B. A. Remington, F. Weber, and S. V. Weber, Phys. Rev. Lett. **76**, 3574 (1996).
8. S. G. Glendinning, S. N. Dixit, B. A. Hammel, D. H. Kalantar, M. H. Key, J. D. Kilkenny, J. P. Knauer, D. M. Pennington, B. A. Remington, R. J. Wallace, and S. V. Weber, Phys. Rev. E **54**, 4473 (1996).
9. R. J. Taylor *et al.*, Phys. Rev. Lett. **76**, 1643 (1996).
10. H. Azechi *et al.*, Phys. Plasmas **4**, 4079 (1997).
11. C. J. Pawley *et al.*, Phys. Plasmas **4**, 1969 (1997).
12. S. G. Glendinning, S. N. Dixit, B. A. Hammel, D. H. Kalantar, M. H. Key, J. D. Kilkenny, J. P. Knauer, D. M. Pennington, B. A. Remington, J. Rothenberg, R. J. Wallace, and S. V. Weber, Phys. Rev. Lett. **80**, 1904 (1998).
13. T. R. Boehly, D. L. Brown, R. S. Craxton, R. L. Keck, J. P. Knauer, J. H. Kelly, T. J. Kessler, S. A. Kumpan, S. J. Loucks, S. A. Letzring, F. J. Marshall, R. L. McCrory, S. F. B. Morse, W. Seka, J. M. Soures, and C. P. Verdon, Opt. Commun. **133**, 495 (1997).
14. K. A. Brueckner and S. Jorna, Rev. Mod. Phys. **46**, 325 (1974).
15. S. V. Weber, S. G. Glendinning, D. H. Kalantar, M. H. Key, B. A. Remington, J. E. Rothenberg, E. Wolfrum, C. P. Verdon, and J. P. Knauer, Phys. Plasmas **4**, 1978 (1997).
16. R. J. Taylor *et al.*, Phys. Rev. Lett. **79**, 1861 (1997).
17. V. A. Smalyuk, T. R. Boehly, D. K. Bradley, J. P. Knauer, and D. D. Meyerhofer, Rev. Sci. Instrum. **70**, 647 (1999).
18. S. W. Haan, Phys. Rev. A **39**, 5812 (1989).
19. V. A. Smalyuk, T. R. Boehly, D. K. Bradley, V. N. Goncharov, J. A. Delettrez, J. P. Knauer, D. D. Meyerhofer, D. Oron, and D. Shvarts, Phys. Rev. Lett. **81**, 5342 (1998); V. A. Smalyuk, T. R. Boehly, D. K. Bradley, V. N. Goncharov, J. A. Delettrez, J. P. Knauer, D. D. Meyerhofer, D. Oron, D. Shvarts, Y. Srebro, and R. P. J. Town, Phys. Plasmas **6**, 4022 (1999).
20. Y. Lin, T. J. Kessler, and G. N. Lawrence, Opt. Lett. **20**, 764 (1995).
21. S. P. Regan, J. Marozas, J. H. Kelly, T. R. Boehly, W. R. Donaldson, P. A. Jaanimagi, R. L. Keck, T. J. Kessler, D. D. Meyerhofer, W. Seka, S. Skupsky, and V. A. Smalyuk, "Experimental Investigation of Smoothing by Spectral Dispersion," submitted to the Journal of the Optical Society of America B. This article also appears in Laboratory for Laser Energetics Review **79**, 149, NTIS document No. DOE/SF/19460-317 (1999). Copies may be obtained from the National Technical Information Service, Springfield, VA 22161.
22. Y. Kato, unpublished notes from work at LLE (1984); Laboratory for Laser Energetics LLE Review **45**, 1, NTIS document No. DOE/DP40200-149 (1990). Copies may be obtained from the National Technical Information Service, Springfield, VA 22161.
23. T. R. Boehly, V. A. Smalyuk, D. D. Meyerhofer, J. P. Knauer, D. K. Bradley, R. S. Craxton, M. J. Guardalben, S. Skupsky, and T. J. Kessler, J. Appl. Phys. **85**, 3444 (1999).
24. R. L. McCrory and C. P. Verdon, in *Inertial Confinement Fusion*, edited by A. Caruso and E. Sindoni (Editrice Compositori, Bologna, Italy, 1989), p. 83.
25. D. Shvarts, U. Alon, D. Ofer, R. L. McCrory, and C. P. Verdon, Phys. Plasmas **2**, 2465 (1995).